Density and confinement effects on fluid velocity slip

Carlos Corral-Casas ©,* Yichong Chen ©, Matthew K. Borg ©, and Livio Gibelli ©†
Institute for Multiscale Themofluids, School of Engineering, The University of Edinburgh,
Edinburgh EH9 3FB, United Kingdom

Understanding the velocity slip of fluids in channels of molecular length scales is essential for accurately manipulating their flow in engineering applications, such as in water desalination or, by reversing the process, osmotic power generation. This study addresses two major open questions, namely (a) the range of validity of the Navier-Stokes equations with slip boundary conditions in describing fluid flows within channels of molecular confinement, and (b) the effect of fluid density and confinement as well as surface properties, such as microscopic roughness and curvature, on fluid slippage along walls. Using a hard-sphere fluid model and describing the fluid-wall interactions by the Maxwell scattering kernel, an event-driven molecular dynamics simulation study was performed in planar and cylindrical channels of different sizes and accommodation coefficients with varying fluid densities. The results show that the well-known criterion for the slip solution, which is valid in rarefied conditions, also holds for a dense gas, i.e., the predictive accuracy improves with decreasing Knudsen numbers, as long as the channel size is larger than about ten molecular diameters. We also find that the key quantity influencing the friction coefficient of a fluid is the peak density at the walls, rather than the nominal density, the fluid confinement, or the channel curvature, as found in previous studies. In particular, higher nominal densities lead to higher density peaks, and therefore a decrease in slip, while tighter confinements lead to lower density peaks, and therefore an increase in slip, regardless of channel geometry. Furthermore, the velocity slip depends on the microscopic roughness via the Smoluchowski factor. These findings are a stepping stone towards a deeper understanding of the molecular mechanisms underlying fluid velocity slip in molecular-scale channels.

I. INTRODUCTION

The study of isothermal gas flows in small channels has been instrumental in the development of micro-electro-mechanical devices (MEMS) [1]. In these systems, gases flow through channels that are only a few micrometres wide, so that the mean free path λ, or the average distance between collisions for gas molecules, approaches the same order of the flow characteristic length of the channel, L. As a result, gas particles begin to collide more frequently with the walls of the system and less frequently with other particles, which means that they deviate from the quasi-local

*c.corral-casas@imperial.ac.uk
†Corresponding author: livio.gibelli@ed.ac.uk

thermodynamic equilibrium assumption of continuum fluid dynamics [2], where the degree of nonequilibrium is quantified by the Knudsen number, $\mathrm{Kn} = \lambda/L$. The Boltzmann equation provides an accurate description of these dilute gas flows over the whole range of Kn, but its asymptotic solution shows that the Navier-Stokes equations can also be applied [3] for slight nonequilibrium conditions, where $\mathrm{Kn} \lesssim 0.1$, provided that the gas is allowed to slip along the surface. The velocity slip at the wall is typically expressed as the product of the slip length times the velocity gradient normal to the wall, where the former is simply proportional to the mean free path by a constant factor known as the slip coefficient [4].

Recent advances in technology have led to a shift in focus from the microscale to the nanoscale [5,6]. In nanoscale engineering applications, the flow characteristic length becomes similar to the diameter of the fluid particles σ, which has significant implications, such as the fact that the quasilocal thermodynamic equilibrium assumption may not hold even at relatively high fluid densities. Under these conditions, the behavior of the fluid becomes dependent on the complex interplay between dense effects ($\lambda \sim \sigma$) and tight geometries ($L \sim \sigma$), which leads to spatial inhomogeneities with preferential ordering in the density profile near the boundaries [7], as well as a material depletion in the central homogeneous region when compared to the nominal density [8]. A notable example of the unexpected fluid behavior that occurs within channels of molecular confinement is that the pressure-driven mass flow rate is found to increase monotonically with decreasing fluid density [9,10], rather than forming a minimum as it does for dilute gas flows [11,12].

While experiments can provide some insight into nanoscale fluid transport [13–15], molecular-based approaches, such as the Enskog equation or molecular dynamics (MD), are better suited to unravel the physics of fluids at the nanoscale [16–19]. In these studies, it has been found that the fluid structuring extends throughout the entire channel when the confinement is very tight ($L/\sigma \lesssim 10$), making the continuum approximation inapplicable. In such extreme conditions, a hydrodynamic-like approach is still possible, but requires the transport coefficients to be spatially dependent and even nonlocal if the channel is only a few molecular diameters in size [20,21].

On the other hand, if the fluid confinement is relatively moderate ($L/\sigma \gtrsim 10$), the conventional Navier-Stokes equations with slip boundary conditions may be valid for some fluid densities, but with some caveats. In particular, the bulk viscosity must be used instead of the nominal viscosity as for unconfined fluids [22] (see Fig. 1 for a visual comparison of these two values), but this introduces uncertainty as the bulk viscosity is not known *a priori* and depends on the confinement of the fluid. Furthermore, the slip length now depends on both the fluid state and the wall in a highly nontrivial way, e.g., the slip length is affected by the fluid structure induced in the directions parallel to the walls [23] and, beyond a threshold, becomes a nonlinear function of the strain rate at the wall [24]. Wetting phenomena [25], the hydrophobic and hydrophilic nature of walls [26], and surface macroscopic roughness [27] have also been found to play a role. Over the years, several models have been developed to describe the slip length from a molecular perspective, including the variable density Frenkel-Kontorova model [28,29] and expressions based on the so-called molecular kinetic theory [30,31], among a myriad of other derivations [32–34].

In this work we aim to address two fundamental questions about molecular-confined fluids that remain elusive despite extensive research: (a) to formulate a quantitative validity criterion for the solution of the Navier-Stokes equations with slip boundary conditions, and (b) to determine the dependence of the fluid slippage on the density and confinement of the fluid, as well as on the surface curvature and microscopic roughness. The first question has not been examined in the literature and it is uncertain whether the criterion established for dilute gases at the microscale, based on the Knudsen number, is applicable to dense, nanoscale-confined fluids. The second question is crucial for resolving the inconsistencies observed in the results of studies on planar and cylindrical geometries, with some suggesting that curvature is the primary factor controlling slip length [35,36], while others show different results [37]. To address the above questions, we have considered a fluid composed of hard-spheres interacting with walls through the Maxwell scattering kernel. Although this modeling approach does not capture all the details of realistic fluid-wall interactions, it can provide valuable insights into the velocity slip by unravelling the essential features with the
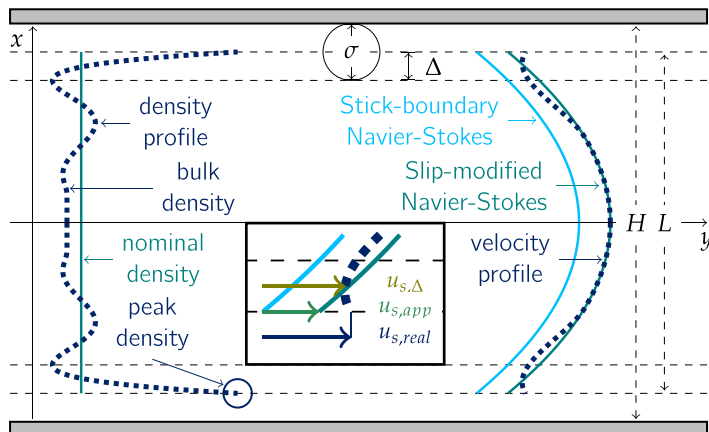
FIG. 1. The schematic depicts a planar channel with nominal height H and characteristic length $L = H - \sigma$, with typical density (left) and velocity (right) profiles. The density profile shows the structuring of the fluid close to the walls, with the first dip marking the boundary of the Δ layer, which is approximately one molecular diameter away from the walls. As highlighted in the inset, three different velocity slips can be defined, namely as the mean velocity in the Δ layer, assuming that the density there is constant $u_{s,\Delta}$, the apparent velocity at the boundary which gives the Navier-Stokes velocity profile in the fluid bulk $u_{s,\mathrm{app}}$, and the real fluid velocity at the boundary $u_{s,\mathrm{real}}$.

most relevant impact. An extensive simulation campaign was then carried out using event-driven molecular dynamics (EDMD), in two geometries (i.e., planar and cylindrical channels) with varying microscopic roughness (as described by the tangential momentum accommodation), and a wide range of fluid rarefaction and confinement conditions. Complementary MD simulations for argon confined between platinum surfaces were performed to show that the main results hold for more realistic systems.

The remainder of the paper is organized as follows. In Sec. II we outline the theoretical treatment and the different computational methods used to numerically evaluate the fluid velocity slip. In Sec. III we present the key findings of our research, whereas in Sec. IV we provide an overview of the significance of our work and future directions for research.

II. METHODOLOGY

A. Slip boundary conditions

The streamwise component of the velocity u_y of a fluid flowing in a planar channel can be described by the Stokes equation

$$\frac{\partial^2 u_y}{\partial x^2} = -\frac{nF_0}{\mu},\tag{1}$$

where x is the coordinate normal to the wall, n and μ are the bulk fluid number density and shear viscosity, respectively, and F_0 is the external force per molecule, which can be interpreted as the pressure gradient $-dP/dy$ acting on the fluid, normalized by the nominal number density.

The governing expression, Eq. (1), must be supplemented with a boundary condition. A first possibility, which seems very natural for a fluid under molecular confinement, is that presented in Ref. [38]. This is an integral boundary condition that defines the velocity slip u_s as the center-of-mass velocity of a thin layer of fluid of constant density and finite width Δ near the wall, which we will call the Δ layer. The width of the Δ layer is defined as the distance from the wall where the

first density oscillation dip occurs, which varies approximately in the range $[\sigma/2, \sigma]$ as the density of the fluid decreases (see Fig. 1). The corresponding integral boundary conditions are

$$u_{s,\Delta}^{-} = \frac{1}{\Delta} \int_{-L/2}^{-L/2+\Delta} u_y \, dx \qquad \text{at the lower wall,} \tag{2a}$$

$$u_{s,\Delta}^{+} = \frac{1}{\Delta} \int_{L/2-\Delta}^{L/2} u_y \, dx \qquad \text{at the upper wall,} \tag{2b}$$

where, by symmetry, $u_{s,\Delta}^{-} = u_{s,\Delta}^{+} = u_{s,\Delta}$. Alternatively, one can adopt the Neumann boundary condition for partial slip as derived by Navier [39] involving the so-called apparent slip velocity, commonly used for dilute gases, which linearly relates the tangential component of the velocity field to the strain rate normal to the wall

$$u_{s,\mathrm{app}}^{\mp} = \pm L_s \frac{\partial u_y}{\partial x}\bigg|_{x=\mp L/2}, \tag{3}$$

where L_s is the slip length.

The solution to the boundary value problems, Eqs. (1) and (2) or Eqs. (1) and (3), reads

$$u_y(x) = \frac{nF_0}{2\mu}\left(-x^2 + \frac{L^2}{4} - \frac{L\Delta}{2} + \frac{\Delta^2}{3}\right) + u_{s,\Delta} = \frac{nF_0}{2\mu}\left(-x^2 + \frac{L^2}{4}\right) + u_{s,\mathrm{app}}, \tag{4}$$

and the following one-to-one correspondence can thus be found between the two different velocity slips (see also the inset in Fig. 1, which illustrates the relationship between $u_{s,\Delta}$ and $u_{s,\mathrm{app}}$, both of which differ from the actual velocity slip at the wall, $u_{s,\mathrm{real}}$)

$$u_{s,\Delta} = u_{s,\mathrm{app}} + \frac{nF_0}{2\mu}\left(\frac{L\Delta}{2} - \frac{\Delta^2}{3}\right). \tag{5}$$

A model for $u_{s,\Delta}$ can be derived by considering the balance of momentum on the Δ layer [38]. The forces acting on this region include the damping force from the wall, the shearing force from the overlying fluid, and the total external force driving the flow. Accordingly, the momentum balance is

$$m_s \frac{du_{s,\Delta}^{-}}{dt} = -\zeta_{0,\Delta} u_{s,\Delta}^{-} + A\mu \frac{\partial u_y}{\partial x}\bigg|_{-L/2+\Delta} + N_s F_0, \tag{6}$$

where m_s and N_s are the total mass and number of molecules in the Δ layer, respectively, $\zeta_{0,\Delta}$ is the so-called zero-frequency friction coefficient, and $A = \ell_y \ell_z$ is the surface area of the interface located between the Δ layer and the fluid, where the strain rate should be evaluated. In steady conditions, using the velocity profile given by Eq. (4) and assuming a constant density across the channel, the velocity slip can be derived as

$$u_{s,\Delta} = \frac{nF_0}{2\xi_{0,\Delta}}L, \tag{7}$$

where $\xi_{0,\Delta} = \zeta_{0,\Delta}/A$ is referred to as the interfacial friction coefficient, which relates the transfer of momentum at the boundary with the velocity slip [40]. As shown in Eq. (7), the velocity slip and the friction coefficient are inversely related and can therefore be used interchangeably. Note that a relationship similar to Eq. (7) also relates $u_{s,\mathrm{app}}$ and $\xi_{0,\mathrm{app}}$, as can be inferred by letting Δ go to zero.

The analytical determination of the interfacial friction coefficient is still an open problem, so numerical methods are commonly used. Once the friction coefficient has been found, the velocity slip follows from Eq. (7) and the overall velocity field from Eq. (4). This section presented the slip solution for fluid flow in a planar channel, but a similar solution can be worked out for the fluid flow in a cylindrical channel, as shown in Appendix A.

B. Fluid and geometry characterization

In this work, we consider the steady flow of a fluid composed of N hard spherical particles with diameter σ and molecular mass m confined in two different geometries: a planar channel defined by two parallel plates separated by a distance $H = h + \sigma$, and a cylindrical channel with diameter $D = d + \sigma$. The relevant flow characteristic length L is defined as the effective height h and diameter d of the planar and cylindrical channels, respectively, to account for the finite size σ of the hard spheres [41]; see Fig. 1.

The fluid-wall interactions are described by the Maxwell scattering kernel. Accordingly, a fraction α of the molecules hitting the wall is assumed to be diffusely reemitted into the fluid after thermalisation with the wall, while the remaining $1 - \alpha$ is specularly reflected. The coefficient α can thus be identified with the tangential momentum accommodation coefficient (TMAC) [2].

The fluid behavior is mainly characterized by two dimensionless groups, namely the nominal reduced density $\eta_0 = n_0 \pi \sigma^3 / 6$, where n_0 is the nominal number density, and the confinement ratio $R = L/\sigma$. The reduced density indicates the number of fluid particles in the theoretical volume occupied by one molecule, and is used to measure the packing fraction, thus distinguishing between dense (high η) and dilute (low η) fluid flows. On the other hand, the confinement ratio is a measure of the channel size, which, in turn, determines the extent of fluid inhomogeneities. As discussed in more detail in Sec. III C, larger values of R correspond to stronger ordering in the fluid near the surface and therefore a more pronounced density peak, whereas lower values of R are associated with a greater density depletion compared to the nominal density in the central region of the channel. The Knudsen number can be expressed in terms of the two dimensionless groups above

$$\mathrm{Kn}(\eta, R) = \frac{\lambda}{L} = \frac{16}{5\pi} \frac{\mu}{P} \sqrt{\frac{\pi kT}{2m}} \frac{1}{L} = \frac{\mu_f(\eta)}{6\sqrt{2}\eta Z(\eta)R}, \tag{8}$$

where η refers to the bulk reduced density, which is smaller than the nominal one in confined geometries; see Fig. 1. The definition of the mean free path is based on the shear viscosity μ for a fluid of hard spheres, whose second-order Enskog approximation reads [2]

$$\mu = \frac{5}{16\sigma^2} \sqrt{\frac{mkT}{\pi}} \mu_f = \frac{5}{16\sigma^2} \sqrt{\frac{mkT}{\pi}} \frac{1}{\chi} \left[1 + \frac{16}{5} \eta\chi + \frac{64}{25} \left(1 + \frac{12}{\pi} \right) \eta^2 \chi^2 \right]. \tag{9}$$

Note that μ_f represents the dense gas correction for the shear viscosity of a rarefied gas, and it depends on the contact value of the pair correlation function χ in uniform equilibrium, which comes from the equation of state for the hard-sphere fluid $P = nkTZ$ [42]

$$\chi = \frac{1}{nb}(Z - 1) = \frac{1}{nb} \left(\frac{1 + \eta + \eta^2 - \eta^3}{(1 - \eta)^3} - 1 \right) = \frac{1}{2} \frac{2 - \eta}{(1 - \eta)^3}, \tag{10}$$

where P is the fluid pressure, k is the Boltzmann constant, T the temperature of the system, Z the fluid compressibility factor, and $b = 2\pi\sigma^3/3$ is the second virial coefficient [2].

C. Simulation setup

The exact time evolution of the hard sphere system is calculated using EDMD [43]. In these simulations, the state of the system jumps from one time to another corresponding to the next collision event by iteratively repeating three basic steps: (a) evaluating the time of the earliest collision event, (b) moving all particles ballistically for that time interval, and (c) updating the velocities of the particles that have collided with another particle or the wall, according to the laws of elastic hard-sphere dynamics or the Maxwell scattering kernel, respectively. It is important to note that the time step is not constant throughout the simulation run, as it depends on the positions and velocities of all molecules in the system. To simplify the notation and data analysis, all physical quantities are made dimensionless in the rest of the paper by considering the molecular diameter σ as the reference length, the particle mass m as the reference mass, and the thermal velocity

$\sqrt{kT/m}$ as the reference velocity, implicitly assuming T as the reference temperature and kT as the reference energy. As a result of these choices, the dimensionless temperature was set to unity in our simulations, and the scaling factor for the force is kT/σ.

For the planar geometry, the computational domain was a parallelepiped box with dimensions $[H; \ell_y; \ell_z]$ and periodic boundary conditions in the y and z directions, whereas for the cylindrical geometry, the computational domain was a cylindrical box with dimensions $[R; \ell_z]$ and periodic boundary conditions in the z direction. For the planar and cylindrical geometry, the streamline lengths (ℓ_y and ℓ_z, respectively) were chosen to be long enough to avoid end effects, and, for the planar geometry, the spanwise dimension ℓ_z was set to match the desired reduced density η_0. In the cylindrical case, the Maxwell scattering kernel was implemented as described in Ref. [44] to properly account for the surface curvature.

The typical simulation was run with over 2.5×10^4 particles to reduce the size dependence of the system and improve the statistical significance of the computed quantities. The particles were initially placed randomly, with the velocity sampled from the Maxwell-Boltzmann distribution using the Box-Muller algorithm. The reduced density was varied in the range $\eta_0 = [0.01, 0.30]$ and the confinement ratios in $R = [10, 50]$, resulting in Knudsen numbers spanning a wide range of values, i.e., Kn $= [0.008, 1]$. In the Poiseuille (planar channel) and Hagen-Poiseuille (cylindrical channel) fluid flows, a constant external force is applied to the particles. The force was chosen in the range $[0.003, 0.05]$ so that the flow is in the linear regime. This ensured proper dissipation of the added heat through the wall and prevented the temperature profile from being affected by the external force.

III. RESULTS AND DISCUSSION

A. Numerical evaluation of the friction coefficient

Before addressing the two key questions posed in Sec. I, we first calculate the friction coefficient for both planar and cylindrical geometries, over a wide range of nominal reduced densities η_0 and confinement ratios R, for rough surfaces represented using a fully diffuse setting ($\alpha = 1$). We chose to calculate the friction coefficient because it primarily encapsulates information about fluid-wall interactions and does not directly involve bulk properties, as the slip length L_s does through its dependence on the viscosity (i.e., $L_s = \mu/\xi_{0,\text{app}}$). In confined fluids, bulk properties such as viscosity depend in a nontrivial way on the nominal density η_0 and degree of confinement R, making it difficult to disentangle whether changes in slip length are due to variations in bulk or interfacial properties, or both.

The friction coefficient was calculated using two independent approaches. In the first approach, which involves nonequilibrium EDMD simulations, $\xi_{0,\Delta}$ is calculated using Eq. (7) where $u_{s,\Delta}$ is evaluated directly from the velocity field as the mean velocity of the fluid in the Δ layer according to Eq. (2). In the second approach, $\xi_{0,\Delta}$ is calculated as the Laplace transform of the ratio between the force-velocity correlation function (being the force that is exerted by the fluid on the wall, or vice versa) and the velocity-velocity autocorrelation function of the fluid in the Δ layer [38,45]. These correlation functions are obtained from equilibrium EDMD simulations in the zero external force limit. It is important to note that, in our simulations, the fluid-wall interaction model using a step function rather than a continuous potential, such as the Lennard-Jones potential. Consequently, the force exerted by the surface on the fluid in the Δ layer was determined by evaluating the average momentum change of particles colliding with the wall, which differs from the approach described in the original work [38].

The results of the different calculations are shown in Fig. 2(a) for the planar geometry and in Fig. 2(b) for the cylindrical geometry. The relative error of the equilibrium and nonequilibrium predictions with respect to their mean is within 4% for $\eta_0 \geqslant 0.1$, but diverges rapidly for smaller densities (this is more easily observed in Appendix B, where values are presented in tables). This
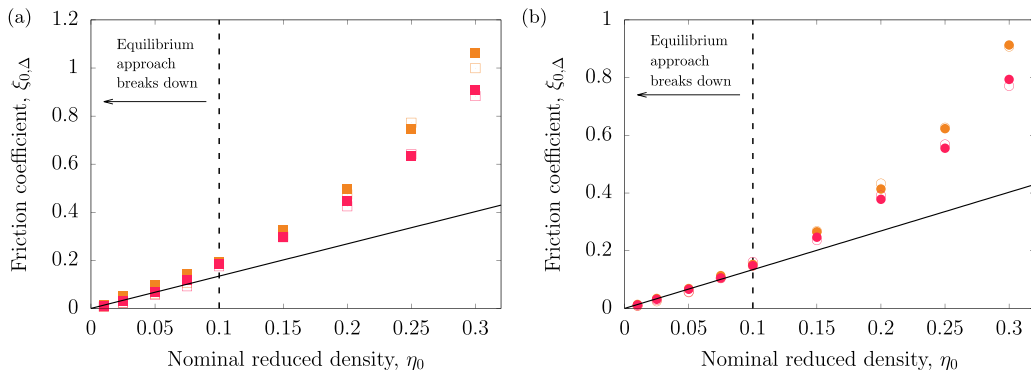
FIG. 2. Interfacial friction coefficients $\xi_{0,\Delta}$ versus the nominal reduced densities for (a) planar and (b) cylindrical channels with fully diffuse walls ($\alpha = 1$). Results are presented for two confinement ratios, $R = 50$ (orange color) and $R = 10$ (red color), produced through nonequilibrium (solid symbols) and equilibrium (empty symbols) approaches. The solid line represents the kinetic theory prediction for rarefied gases, Eq. (11). See Appendix B for results over a wider range of confinement ratios and in tabular form.

is not unexpected since, for more dilute fluids, the density fluctuations do not allow the correlation functions to be evaluated accurately enough [38].

It is worth noting that, for the largest channels (i.e., small curvature effect) and smallest reduced densities (i.e., spatially homogeneous density with a bulk density close to the nominal value), the friction coefficients of both geometries evaluated using the nonequilibrium approach agree with each other, and approach the value predicted by the Boltzmann equation [4]

$$\xi_{0,B} = \frac{15}{8\sigma^3 \bar{c}_1} \sqrt{\frac{2mkT}{\pi}} \eta, \tag{11}$$

where $\bar{c}_1 = 1.1144$ is the (constant) first-order slip coefficient for the hard-sphere Boltzmann equation [46].

B. What is the quantitative criterion for the validity of the slip solution?

The purpose of this section is to address the first key question posed in Sec. I, namely to establish a criterion for the applicability of the slip solution to the description of force-driven fluid flows within molecular confinement. The accuracy of the slip solution was theoretically evaluated by using the velocity field from Eqs. (4) and (A4) for planar and cylindrical channels, respectively, with the apparent velocity slip estimated from non-equilibrium simulations as described in Sec. III A, for fully diffuse walls ($\alpha = 1$). In these expressions, the curvature of the velocity profile (i.e., the coefficient of the quadratic term) was obtained by fitting the numerical velocity profile provided by nonequilibrium EDMD simulations, rather than being calculated directly from the bulk properties of the fluid. This was necessary because the direct numerical evaluation of the velocity curvature using bulk values of density and viscosity is prone to numerical inaccuracies, which have been found to be up to 15% in the worst case. In fact, as shown in Eq. (4), the velocity curvature depends on the viscosity, which is a highly nonlinear function of the density, see Eq. (9), but the accurate estimation of the density is challenging, especially for large channels where a small force must be applied to keep the flow in the linear regime.

The results of this investigation are presented in Figs. 3(a) and 3(b) for planar and cylindrical channels, respectively. In order to decide whether the slip solution was accurate or not, we calculated the root mean square error between the EDMD velocity profile (target) and the velocity profile given by the analytical solution, Eq. (4) or (A4) (prediction). Both profiles were divided by the maximum of the EDMD velocity profile to ensure a consistent error scale across different conditions. The
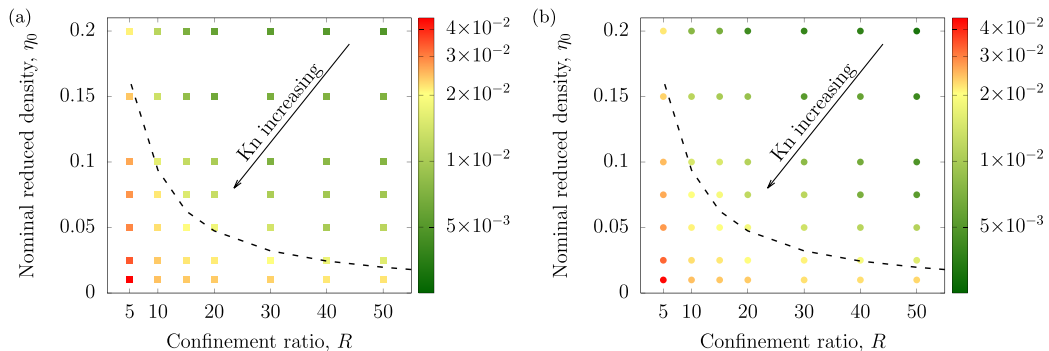
FIG. 3. Accuracy of the slip solution for (a) planar and (b) cylindrical channels with fully diffuse walls ($\alpha = 1$). The color scale bar shows the root mean square error between the numerical velocity profile and the slip analytical prediction. The error increases from green (lowest) to red (highest). The dashed lines represent the fluid conditions corresponding to $Kn = 0.1$, above which the slip solution gives errors below 0.02 for $R \gtrsim 10$.

data points are shaded from green to red as the value of the computed error increases. It can be seen that the accuracy of the slip solution degrades gradually as either R or η decreases, so no sharp threshold can be defined for its validity. Nevertheless, for $Kn \leqslant 0.1$ (above the dashed lines in Fig. 3) the slip solution can be considered accurate since the root mean square error is less than 0.02, unless the confinement is very tight, in which case it turns out to be inaccurate for all Kn (see, for example, the results for $R = 5$). This is not unexpected as nonlocal effects of molecular interactions become increasingly important as R decreases and eventually cause the Navier-Stokes equations to fail [21,47]. This situation differs from the more extensively studied rarefied gas scenario, where the failure of the hydrodynamic approach is primarily due to the increasing number of fluid-wall interactions, which are fully represented by Kn [4]. The key point from Fig. 3 is that, although the interfacial friction coefficient can be calculated for fluids of any density and confined within any channel size, its use within the Navier-Stokes framework (through the slip boundary conditions) provides velocity profiles that become increasingly inaccurate as either R or η decreases. This is why, in the following, only the slip solutions corresponding to the numerical results for $Kn \leqslant 0.1$ and $R \geqslant 10$ are considered.

C. How does the friction coefficient depend on the density and confinement of the fluid, and on the curvature and roughness of the walls?

The purpose of this section is to address the second key question posed in Sec I, namely how the density and confinement of the fluid, alongside the curvature of the channel and roughness of the walls, affect the friction coefficient. The main point to note is that the friction coefficient represents the transfer of tangential momentum between the fluid and the surface [40], and in our simple simulation setup this transfer can only occur when particles hit the surface. As we have verified in our simulations, the frequency of fluid-wall collisions is directly proportional to the density peak at the wall, and therefore a linear relationship between the friction coefficient and the density peak would be expected. The density peak is defined here as the maximum value of the density reached in the outermost cell accessible to the center of the hard spheres, which is located at a distance of a molecular radius $\sigma/2$ from the wall (see also Fig. 1). In other work, such a relationship has been derived under certain assumptions and supported by MD simulations for a Lennard-Jones fluid with realistic walls [25,31,32]. However, the average density in the Δ layer was used rather than the peak density, which we believe to be more relevant, as discussed below. More importantly, conflicting
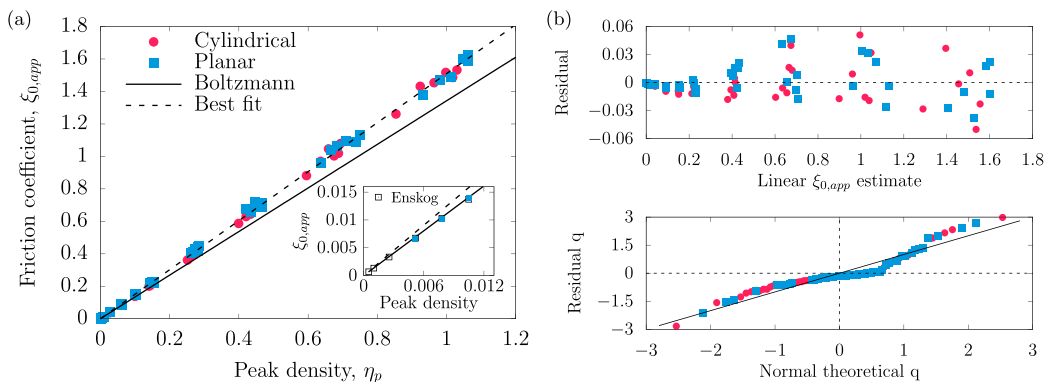
FIG. 4. (a) Friction coefficient versus peak density for planar (blue squares) and cylindrical (red circles) channels with fully diffuse walls ($\alpha = 1$). (b) Residuals and $Q - Q$ plots. Of the numerical results presented in Fig. 3, only those corresponding to conditions where the slip solution accuracy is met (i.e., root mean square error lower than 0.02) are shown here. The dashed black line in panel (a) represents the best linear fit of the results, while the solid black line represents the kinetic theory prediction for rarefied gases, Eq. (11). The inset zooms into this regime in the lower left.

results have been reported, with some suggesting a linear correlation [25,31] and others suggesting a power-law relationship with an exponent other than unity [32].

Figure 4(a) clearly shows that, in the case of full accommodation, the friction coefficient scales linearly with the density peak in both planar and cylindrical channels, regardless of the nominal fluid density, confinement ratio and wall curvature. Two remarks are in order. First, using the average density in the Δ layer instead of the peak density would result in a nonlinear relationship, showing that the peak density is more closely related to the friction coefficient. Second, the observation that the density peak is linearly proportional to the friction coefficient, independent of the confinement, is not restricted to the hard sphere model used in this study, as confirmed by complementary MD simulations we performed on argon gas confined between platinum walls in a planar geometry. The detailed description of these simulations is given in Appendix C. The goodness of the linear fit shown in Fig. 4(a) is indicated by the low value of the chi-square $\mathcal{X}^2 \approx 0.0391$ statistic and the high value of the $\mathcal{R}^2 \approx 0.999$ correlation index, and is further supported by the analysis of the residuals and the $Q - Q$ scatter plot shown in Fig. 4(b). The lack of a clear pattern in the residuals and the fairly good alignment along the bisector of the first quadrant of the $Q - Q$ scatter plot indicate that the residuals are approximately normally distributed, as they should be for an ideal linear fit. Specifically, the residual analysis tests two regression assumptions, namely random scatter around zero and constant error variance across the independent variable. The quantile-quantile plot evaluates the Gaussian distribution of the residuals by plotting the residual quantiles against the theoretical ones. A linear pattern through the origin with a unitary slope indicates normality, while upward sloping curves indicate heavier tails, downward sloping curves indicate lighter tails, and nonlinearities in the middle indicate skewness relative to the Gaussian distribution.

As can be seen more clearly in the inset of Fig. 4(a), the proposed linear fit of the results is not entirely accurate in the limit of low density. In fact, its slope does not match the slope predicted by the Boltzmann equation, Eq. (11), as it should for these small reduced densities (note that under these conditions the peak density coincides with the nominal density). The relationship between the friction coefficient and peak density is also plotted as predicted by the Boltzmann equation for arbitrary densities in the main plot. Interestingly, the ratio of the slope of this curve to that of the curve fitted by EDMD results is very well given by a numerical factor of $\sqrt{\pi}/2$.

EDMD simulations in dilute conditions are computationally intensive, so we further support this conclusion by solving the Enskog equation, which gives equivalent results to EDMD in the low
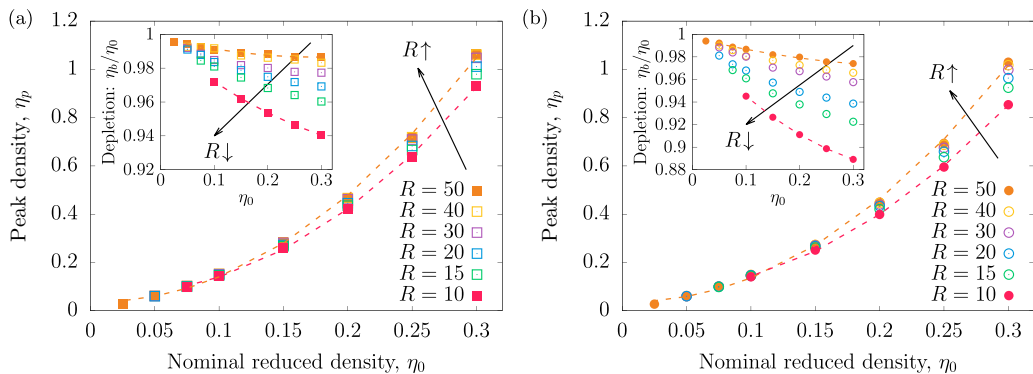
FIG. 5. Comparison of the peak density next to the wall and the nominal reduced density within (a) planar and (b) cylindrical channels for different confinement ratios with fully diffuse walls ($\alpha = 1$). The insets show the density depletion in the middle of the channel.

density limit [see empty squares in the inset of Fig. 4(a)]. The Enskog equation was solved with an independent code that implements a particle method [48]. Even Enskog solutions fit perfectly the linear relationship predicted by the Boltzmann equation and deviate from the proposed linear fit (dashed line). This clearly shows that the discrepancy is due to the proposed fit and not, as one might have thought, to nonlocal effects which, unlike the Boltzmann equation, are included in the Enskog equation even in the low density regime. Note, however, that these deviations are minimal, so the proposed linear fit is still a good engineering approximation in the entire range of nominal fluid densities.

As Fig. 4(a) clearly shows, the friction coefficient is primarily determined by the peak density. Channel curvature and confinement influence the friction coefficient only indirectly by modifying the peak density. This key finding helps to rationalize the results of previous studies, which have investigated the effects of nominal density [37], fluid confinement [19], and channel curvature [35,36] on the friction coefficient, without explicitly referring to the peak density, and have sometimes reached conflicting conclusions. For example, Refs. [35,36] concluded that the curvature, and not the degree of confinement, controls the friction coefficient, in contrast to the results of Ref. [37], which show different friction coefficients within planar geometries when the confinement is varied. According to our results, the friction coefficient decreases because (for a given nominal density) with tighter confinement the peak density decreases [49], regardless of the channel curvature and the wall roughness.

This conclusion is clearly shown in Fig. 5, where the density peak is plotted against the nominal density. For both planar and cylindrical channels, it is observed that the peak density increases quadratically with the nominal density at constant confinement. Likewise, at constant density, higher degrees of confinement (i.e., lower R values) result in smaller density peaks (in the fittings shown by dashed lines, $\mathcal{X}^2 \lessapprox 0.057$ and $\mathcal{R}^2 \gtrapprox 0.997$). This can be explained by the fact that the bulk density becomes increasingly smaller than the nominal density as the degree of confinement increases [8], as can be seen in the two insets of Fig. 5. As a result, the net force pushing the atoms towards the walls [48], which is proportional to the bulk density, decreases and so does the peak density. It is found that the relationship between the nominal density and the peak density is well approximated by a polynomial fit, which, for instance, in the cylindrical geometry reads

$$\eta_p = (0.0515R + 7.7012)\eta_0^2 + (-0.0033R + 0.5228)\eta_0, \tag{12}$$

with a relative error of less than 10% for $\eta_0 \gtrapprox 0.1$.

Finally, we consider the case of walls with a smaller microscopic roughness, or equivalently a smaller α. Figure 6 shows that the friction coefficient remains a linear function of the peak
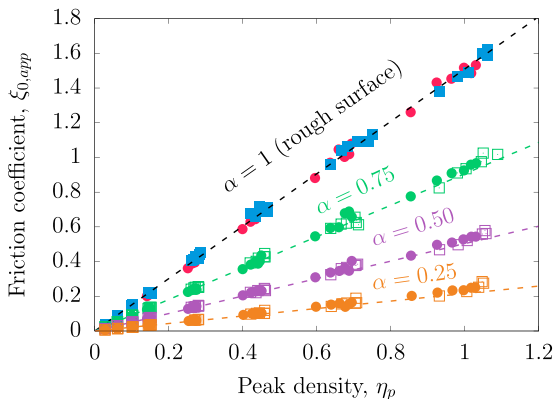
FIG. 6. Friction coefficient versus peak density for different wall accommodation coefficients. As in the fully diffuse case, results do not depend on the channel geometry for partial TMAC (planar geometries are represented with empty symbols as a guide to the eye). Colored dashed lines are obtained by scaling the dashed black line, from Fig. 4(a) corresponding to the full accommodation case, with the Smoluchowski prefactor.

density, with the results for planar and cylindrical channels superimposed. The peak density does not depend on α, but the friction coefficient is found to decrease with it according to the inverse Smoluchowski prefactor $\alpha/(2-\alpha)$, as is the case under dilute conditions. Note that the dependence of the friction coefficient on α is not unexpected, since, for the same collision frequency of particles with walls, the transfer of tangential momentum between fluid and wall becomes less efficient as the accommodation coefficient decreases. However, this finding further validates our results. Indeed, the scaling based on the Smoluchowski factor was mathematically derived in rarefied conditions, but if a linear relationship between the friction coefficient and peak density holds, the same factor should also allow the results to be rescaled in the dense regime.

The results shown in Figs. 4–6 together allow us to answer the question posed at the beginning of Section III C. For a given confinement ratio, the peak density increases significantly as the nominal density increases, especially for looser confinement of the fluid (Fig. 5). Accordingly, the interfacial friction coefficient increases [Fig. 4(a)], and so the velocity slip decreases. Conversely, for a given nominal density, the peak density decreases as the confinement becomes tighter, especially at higher densities (insets of Fig. 5 showing the depletion in the middle region of the channel), resulting in a decrease in the friction coefficient and an increase in the velocity slip. Finally, the friction coefficient is independent of the wall curvature and decreases with the Smoluchowski factor as one moves from rough to smooth surfaces, decreasing the TMAC value (Fig. 6). Note that in realistic systems it may be the case that a change in wall curvature leads to a smoother energy landscape of fluid-wall interactions, which is equivalent to a lower TMAC and, therefore, a decrease in the friction coefficient [35].

It should be emphasized that the slip phenomenon is often treated on the basis of transition state theory. According to this theory, molecules adjacent to walls jump between free sites by overcoming an energy barrier determined by fluid-wall interactions, also identified with the microscopic roughness. Macroscopic slip occurs when these jumps occur in a preferred direction. As the confinement becomes tighter, velocity slip increases because microscopic roughness decreases, and molecules jump more frequently along the wall sites. This picture is typically supported by MD [19,29,35,37]. Our simplified approach has revealed that additional factors are at play by allowing independent control of confinement (by adjusting the channel size, R) and roughness (by adjusting the tangential momentum accommodation coefficient, α), which is not possible in classical MD involving molecular walls. In particular, we showed that even when the microscopic roughness is kept constant, variations in velocity slip can occur due to changes in confinement. In fact, for

constant α (and nominal density), reducing R decreases the density peak, which in turn causes the velocity slip to increase. Since the density peak is formed by the net force pushing the particles from the bulk fluid towards the wall, the observed decrease in friction under confinement can also be attributed to fluid-fluid interactions and not solely to reduced energy barriers between wall sites. Therefore, our model demonstrates that fluid-fluid interactions, beyond fluid-wall interactions, play an overlooked role in friction, and clarifies the mechanical process by which this occurs. Such a finding highlights the unique insights provided by our more fundamental approach.

IV. CONCLUSIONS

The aim of this study was to investigate the velocity slip of fluids in molecular-scale channels, in particular the validity of the Navier-Stokes equation with slip boundary conditions. This study used a hard-sphere fluid model and performed an event-driven molecular dynamics simulation study, varying fluid properties, confinement degree, geometry, and surface microscopic roughness.

The results for both planar and cylindrical channels clearly showed that the effect of surface curvature alone is negligible and that the friction coefficient (or, equivalently, the velocity slip) depends on two mechanisms. The first is the collision frequency of the molecules with the wall, which determines the "gross" momentum transfer, i.e., the amount of momentum potentially transferable to the walls. The second is the microscopic roughness of the walls, which determines the "net" momentum transfer, i.e., the amount of momentum actually transferred to the walls. Specifically, we found that the fluid-wall collision frequency depends linearly on the density peak that occurs adjacent to the boundary, rather than on the nominal fluid density or the confinement ratio individually. Note that this linear relationship is not an artifact of the hard-sphere model used in our study, as it is confirmed by complementary MD simulations of argon gas on platinum walls. On the other hand, in our simulation setup, the microscopic roughness is simply modulated by the accommodation coefficient.

Our study found that the slip solution criterion valid for dilute conditions also holds for dense gases as long as the fluid is only moderately confined. That is, the Knudsen number must be less than $\mathrm{Kn} \lesssim 0.1$ and the confinement must be greater than $R \gtrsim 10$ for the Navier-Stokes equations with slip boundary conditions to provide an accurate description of the fluid flow.

Our study also found that

(i) For a fixed confinement ratio, the friction coefficient (velocity slip) increases (decreases) with increasing nominal density. This is because a higher density results in a larger fluid layering on the walls, and therefore a higher fluid-wall collision frequency that hinders fluid slippage.

(ii) For a fixed density, the friction coefficient (velocity slip) increases (decreases) with larger confinement ratios. This is because a tighter confinement leads to a smaller fluid layering on the walls, and therefore a lower fluid-wall collision frequency that promotes fluid slippage.

(iii) The friction coefficient is independent of the wall curvature and decreases according to the inverse Smoluchowski prefactor as one moves from rough to smooth surfaces.

These results, which are visually summarized in Fig. 7, provide valuable insights into the physics of confined fluids and represent an important step towards understanding the molecular mechanisms behind fluid velocity slip in molecular-sized channels. Future research directions could include a more systematic probe of how the complexity of the fluid model, such as molecules interacting through continuous potentials, as well as more realistic fluid-wall interactions, affect fluid slippage at walls. This would help to resolve the current inconsistencies in the velocity slip literature and clarify the physical origins of such phenomena.
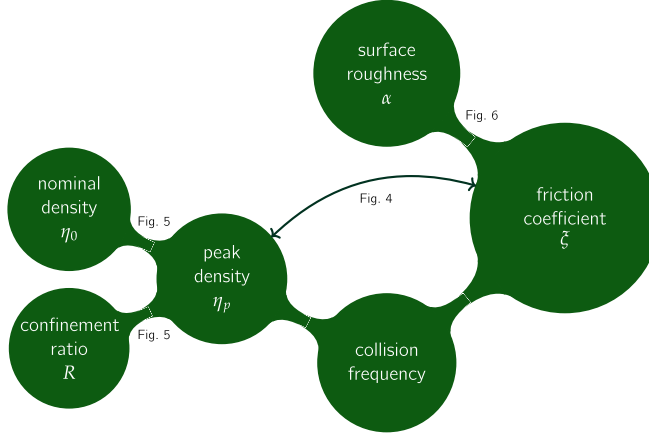
ACKNOWLEDGMENT

FIG. 7. Summary of the main results from this work, showing schematically how specific fluid and wall properties ultimately influence the friction coefficient. Relationships can be seen through some of the figures in the paper, as indicated in the connections between entities.

APPENDIX A: THE HAGEN-POISEUILLE FLOW WITH SLIP

The equation for fluid flow in a cylindrical pipe with axis z using the Stokes equation in cylindrical coordinates is written as

$$\frac{1}{r}\frac{\partial}{\partial r}\left(r\frac{\partial u_z}{\partial r}\right) = -\frac{nF_0}{\mu}, \tag{A1}$$

where u_z is the axial velocity component and r is the radial distance from the central streamline axis of the cylindrical channel. The integral boundary condition complementing the governing equation is

$$u_{s,\Delta} = \frac{2}{\Delta(L-\Delta)}\int_{L/2-\Delta}^{L/2} r u_z \, dr, \tag{A2}$$

which is equal to the mean velocity of the fluid in the thin shell adjacent to the wall under the assumption of constant density in the Δ layer, while the Navier slip boundary condition reads

$$u_{s,\text{app}} = -L_s\frac{\partial u_z}{\partial r}\Big|_{r=L/2}. \tag{A3}$$

The solution to the boundary value problem, either Eqs. (A1) and (A2) or Eqs. (A1) and (A3), is referred to as the slip-modified Hagen-Poiseuille solution

$$u_z(r) = \frac{nF_0}{4\mu}\left(-r^2 + \frac{L^2}{4} - \frac{L\Delta}{2} + \frac{\Delta^2}{2}\right) + u_{s,\Delta} = \frac{nF_0}{4\mu}\left(-r^2 + \frac{L^2}{4}\right) + u_{s,\text{app}}, \tag{A4}$$

and the following one-to-one correspondence can thus be found between the two different velocity slips

$$u_{s,\Delta} = u_{s,\text{app}} + \frac{nF_0}{4\mu}\left(\frac{L\Delta}{2} - \frac{\Delta^2}{2}\right). \tag{A5}$$

As for the planar geometry, a momentum balance similar to Eq. (6) can be evaluated for the fluid in the annular Δ layer

$$m_s\frac{du_{s,\Delta}}{dt} = -\zeta_{0,\Delta}u_{s,\Delta} + A\mu\frac{\partial u_z}{\partial r}\Big|_{L/2-\Delta} + N_sF_0 = 0, \tag{A6}$$

TABLE I. Planar channels. Comparison of interfacial friction coefficients $\xi_{0,\Delta}$ for nominal reduced densities η_0 and confinement ratios R of interest, using nonequilibrium (left column) and equilibrium (right column) approaches. Walls are fully diffuse ($\alpha = 1$).

η_0	$R = 50$		$R = 40$		$R = 30$		$R = 20$		$R = 15$		$R = 10$	
0.30	1.0604	0.9992	1.0475	1.0023	1.0239	0.9945	0.9726	0.9432	0.9606	0.9153	0.9082	0.8832
0.25	0.7457	0.7721	0.7211	0.7375	0.7037	0.6983	0.6778	0.6874	0.6645	0.6541	0.6336	0.6408
0.20	0.4956	0.4737	0.4801	0.4667	0.4674	0.4542	0.4682	0.4588	0.4480	0.4313	0.4455	0.4248
0.15	0.3258	0.3026	0.3210	0.2963	0.3086	0.2992	0.3090	0.2893	0.3008	0.2843	0.2951	0.2961
0.10	0.1927	0.1857	0.1908	0.1932	0.1892	0.1834	0.1902	0.1787	0.1868	0.1697	0.1837	0.1755
0.075	0.1430	0.1067	0.1438	0.1069	0.1441	0.0952	0.1414	0.0963	0.1382	0.0954	0.1172	0.0924
0.05	0.0960	0.0616	0.0967	0.0542	0.0959	0.0578	0.0947	0.0476	0.0712	0.0568	0.0703	0.0571
0.025	0.0515	0.0239	0.0506	0.0241	0.0353	0.0221	0.0344	0.0266	0.0335	0.0245	0.0323	0.0236
0.01	0.0140	0.0077	0.0137	0.0082	0.0134	0.0086	0.0127	0.0088	0.0121	0.0073	0.0112	0.0071

where now the surface area in the shell-fluid interface depends on the width of the annular layer, $A = \pi(L - \Delta)\ell_z$, being ℓ_z the length of the tube. Accordingly, an inverse relationship between the velocity slip and the friction coefficient can be found again as

$$u_{s,\Delta} = \frac{nF_0}{2\xi_0}\frac{L}{2}. \tag{A7}$$

APPENDIX B: COMPARISON WITH RESULTS OBTAINED IN EQUILIBRIUM SIMULATIONS

The supplementary data presented in Tables I and II complement the main analysis of Sec. III A. As discussed there, the two methods begin to diverge at low reduced densities ($\eta_0 \lesssim 0.1$), where the assumptions behind the equilibrium calculations break down [38,45].

APPENDIX C: MOLECULAR DYNAMICS SIMULATIONS

The observed linear relationship between friction coefficient and density peak shown in Fig. 4(a) is not just an artifact of the hard sphere model used in EDMD, but it persists when more realistic intermolecular interactions are considered. To support this claim, complementary nonequilibrium MD simulations were performed using the open-source LAMMPS software [50]. The simulation setup consisted of monatomic argon (Ar) molecules confined within planar physical walls, defined

TABLE II. Cylindrical channels. Comparison of interfacial friction coefficients $\xi_{0,\Delta}$ for nominal reduced densities η_0 and confinement ratios R of interest, using nonequilibrium (left column) and equilibrium (right column) approaches. Walls are fully diffuse ($\alpha = 1$).

| η_0	$R = 50$		$R = 40$		$R = 30$		$R = 20$		$R = 15$		$R = 10$	
0.30	0.9130	0.9074	0.8965	0.9311	0.8964	0.9189	0.8779	0.8614	0.8633	0.8721	0.7937	0.7712
0.25	0.6231	0.6265	0.6015	0.5952	0.6010	0.6287	0.6133	0.6330	0.5868	0.6104	0.5553	0.5685
0.20	0.4139	0.4328	0.4269	0.4386	0.4106	0.4467	0.3988	0.3952	0.3935	0.4012	0.3783	0.3913
0.15	0.2657	0.2679	0.2668	0.2654	0.2574	0.2621	0.2601	0.2534	0.2567	0.2693	0.2467	0.2365
0.10	0.1524	0.1484	0.1575	0.1457	0.1581	0.1517	0.1572	0.1571	0.1516	0.1412	0.1481	0.1612
0.075	0.1136	0.1053	0.1138	0.1034	0.1080	0.1023	0.1092	0.1097	0.1083	0.1113	0.1054	0.1046
0.05	0.0689	0.0558	0.0700	0.0595	0.0695	0.0648	0.0693	0.0561	0.0688	0.0624	0.0663	0.0571
0.025	0.0344	0.0246	0.0340	0.0257	0.0337	0.0265	0.0335	0.0256	0.0329	0.0269	0.0315	0.0289
0.01	0.0136	0.0086	0.0135	0.0086	0.0132	0.0086	0.0129	0.0103	0.0125	0.0099	0.0117	0.0098
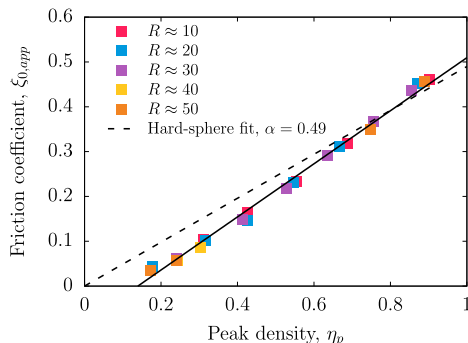
FIG. 8. Friction coefficient versus peak density for MD, in the same range of confinement ratios and nominal densities to those of EDMD simulations. The solid line corresponds to the best linear fit of the MD values, whereas the dashed lines represents the EDMD fit from Fig. 4(a) with the TMAC value from MD simulations ($\alpha = 0.49$).

by platinum (Pt) atoms following a face-centred cubic array with a lattice parameter of 3.92 Å. The distance between the walls was assumed to be H, and periodic boundary conditions were applied in the nonconstraining directions where $L_y = L_z = 400$ Å. The interactions were modeled using the 12-6 Lennard-Jones potential [51] with a cutoff of 15 Å, and the velocity Verlet algorithm with a time step of 1 fs was used to integrate the molecular trajectories. An external force of $F_0 \leqslant 5.5 \times 10^{-14}$ N/atom was applied in the streamwise direction, ensuring that its magnitude was sufficiently small to keep the flow in the linear regime.

Each MD simulation consisted of two steps, equilibration and production. During the equilibration step, the temperature of both the gas and wall atoms was maintained at 300 K using a Nosé-Hoover thermostat with a time constant of 100 fs. After equilibration, the thermostat was turned off on the gas molecules to avoid biasing their slipping behavior. Similarly to EDMD, the quantities in MD simulations were made dimensionless using the reference values $\sigma = 3.35$ Å, $m = 6.63 \times 10^{-26}$ kg and the thermal velocity $\sqrt{kT/m}$, and the friction coefficient was calculated using the procedure described in Sec. III. The TMAC value for the gas-surface interaction was found to be $\alpha = 0.49$, independently of the confinement ratio.

Although the MD simulations refer to a more realistic fluid than EDMD, Fig. 8 shows that a linear relationship between the interfacial friction coefficient and the density peak is still observed. Analysis of the residuals, similar to that shown in Fig. 4(b), from the linear fit in Fig. 8 (solid line) revealed a nonsystematic pattern. This indicates that the linear model provides a good description of the relationship between friction coefficient and peak density for the MD results as well. The differences between the solid and dashed lines in Fig. 8 are not unexpected, and are due to the different intermolecular interactions (Lennard-Jones in MD versus hard sphere in EDMD) and the different scattering of molecules at the walls (real versus stochastic). In fact, although the tangential momentum accommodation coefficient is the same for both MD and EDMD simulations, the friction coefficient is expected to depend on the fine details of how molecules are scattered from the wall, which are different in the two cases. However, these discrepancies do not detract from the remarkable qualitative similarity of the results, which clearly demonstrates the ability of the simpler modeling approach used in this study to provide qualitatively valid results for real-world scenarios.

[1] M. Gad-el Hak, The fluid mechanics of microdevices-The Freeman Scholar Lecture, J. Fluids Eng. **121**, 5 (1999).

[2] G. M. Kremer, *An Introduction to the Boltzmann Equation and Transport Processes in Gases*, 1st ed. (Springer, Berlin, 2010).

[3] N. G. Hadjiconstantinou, The limits of Navier-Stokes theory and kinetic extensions for describing small-scale gaseous hydrodynamics, Phys. Fluids **18**, 111301 (2006).

[4] E. H. Kennard, *Kinetic Theory of Gases, with an Introduction to Statistical Mechanics* (McGraw-Hill, New York, 1938).

[5] W. Sparreboom, A. van den Berg, and J. C. Eijkel, Transport in nanofluidic systems: A review of theory and applications, New J. Phys. **12**, 015004 (2010).

[6] N. Kavokine, R. R. Netz, and L. Bocquet, Fluids at the nanoscale: From continuum to subcontinuum transport, Annu. Rev. Fluid Mech. **53**, 377 (2021).

[7] J. N. Israelachvili, Solvation, structural, and hydration forces, in *Intermolecular and Surface Forces*, 3rd ed., edited by J. N. Israelachvili (Academic Press, Boston, 2011), Chap. 15, pp. 341–380.

[8] G. J. Wang and N. G. Hadjiconstantinou, Why are fluid densities so low in carbon nanotubes? Phys. Fluids **27**, 052006 (2015).

[9] L. Wu, H. Liu, J. M. Reese, and Y. Zhang, Non-equilibrium dynamics of dense gas under tight confinement, J. Fluid Mech. **794**, 252 (2016).

[10] C. Corral-Casas, J. Li, M. K. Borg, and L. Gibelli, Knudsen minimum disappearance in molecular-confined flows, J. Fluid Mech. **945**, A28 (2022).

[11] W. G. Pollard and R. D. Present, On gaseous self-diffusion in long capillary tubes, Phys. Rev. **73**, 762 (1948).

[12] C. Cercignani and A. Daneri, Flow of a rarefied gas between two parallel plates, J. Appl. Phys. **34**, 3509 (1963).

[13] M. Majumder, N. Chopra, R. Andrews, and B. J. Hinds, Enhanced flow in carbon nanotubes, Nature (London) **438**, 44 (2005).

[14] J. K. Holt, H. G. Park, Y. Wang, M. Stadermann, A. B. Artyukhin, C. P. Grigoropoulos, A. Noy, and O. Bakajin, Fast mass transport through sub-2-nanometer carbon nanotubes, Science **312**, 1034 (2006).

[15] M. Whitby, L. Cagnon, M. Thanou, and N. Quirke, Enhanced fluid flow through nanoscale carbon pipes, Nano Lett. **8**, 2632 (2008).

[16] Q. Sheng, L. Gibelli, J. Li, M. K. Borg, and Y. Zhang, Dense gas flow simulations in ultra-tight confinement, Phys. Fluids **32**, 092003 (2020).

[17] G. Hummer, J. C. Rasaiah, and J. P. Noworyta, Water conduction through the hydrophobic channel of a carbon nanotube, Nature (London) **414**, 188 (2001).

[18] A. I. Skoulidas, D. M. Ackerman, J. K. Johnson, and D. S. Sholl, Rapid transport of gases in carbon nanotubes, Phys. Rev. Lett. **89**, 185901 (2002).

[19] J. A. Thomas and A. J. H. McGaughey, Reassessing fast water transport through carbon nanotubes, Nano Lett. **8**, 2788 (2008).

[20] I. Bitsanis, T. K. Vanderlick, M. Tirrell, and H. T. Davis, A tractable molecular theory of flow in strongly inhomogeneous fluids, J. Chem. Phys. **89**, 3152 (1988).

[21] K. P. Travis, B. D. Todd, and D. J. Evans, Departure from Navier-Stokes hydrodynamics in confined liquids, Phys. Rev. E **55**, 4288 (1997).

[22] X. D. Din and E. E. Michaelides, Kinetic theory and molecular dynamics simulations of microscopic flows, Phys. Fluids **9**, 3915 (1997).

[23] P. A. Thompson and M. O. Robbins, Shear flow near solids: Epitaxial order and flow boundary conditions, Phys. Rev. A **41**, 6830 (1990).

[24] P. A. Thompson and S. M. Troian, A general boundary condition for liquid flow at solid surfaces, Nature (London) **389**, 360 (1997).

[25] J. L. Barrat and L. Bocquet, Influence of wetting properties on hydrodynamic boundary conditions at a fluid/solid interface, Faraday Discuss. **112**, 119 (1999).

[26] C. Sendner, D. Horinek, L. Bocquet, and R. R. Netz, Interfacial water at hydrophobic and hydrophilic surfaces: Slip, viscosity, and diffusion, Langmuir **25**, 10768 (2009).

[27] N. V. Priezjev and S. M. Troian, Influence of periodic wall roughness on the slip behaviour at liquid/solid interfaces: Molecular-scale simulations versus continuum predictions, J. Fluid Mech. **554**, 25 (2006).

[28] S. Lichter, A. Roxin, and S. Mandre, Mechanisms for liquid slip at solid surfaces, Phys. Rev. Lett. **93**, 086001 (2004).

[29] A. Martini, A. Roxin, R. Q. Snurr, Q. Wang, and S. Lichter, Molecular mechanisms of liquid slip, J. Fluid Mech. **600**, 257 (2008).

[30] F.-C. Wang and Y.-P. Zhao, Slip boundary conditions based on molecular kinetic theory: The critical shear stress and the energy dissipation at the liquid–solid interface, Soft Matter **7**, 8628 (2011).

[31] G. J. Wang and N. G. Hadjiconstantinou, Universal molecular-kinetic scaling relation for slip of a simple fluid at a solid boundary, Phys. Rev. Fluids **4**, 064201 (2019).

[32] N. V. Priezjev, Rate-dependent slip boundary conditions for simple fluids, Phys. Rev. E **75**, 051605 (2007).

[33] N. G. Hadjiconstantinou, An atomistic model for the Navier slip condition, J. Fluid Mech. **912**, A26 (2021).

[34] N. G. Hadjiconstantinou and M. M. Swisher, On the equivalence of nonequilibrium and equilibrium measurements of slip in molecular dynamics simulations, Phys. Rev. Fluids **7**, 114203 (2022).

[35] K. Falk, F. Sedlmeier, L. Joly, R. R. Netz, and L. Bocquet, Molecular origin of fast water transport in carbon nanotube membranes: Superlubricity versus curvature dependent friction, Nano Lett. **10**, 4067 (2010).

[36] S. K. Kannam, B. D. Todd, J. S. Hansen, and P. J. Daivis, Interfacial slip friction at a fluid-solid cylindrical boundary, J. Chem. Phys. **136**, 244704 (2012).

[37] B. Shan, P. Wang, R. Wang, Y. Zhang, and Z. Guo, Molecular kinetic modelling of nanoscale slip flow using a continuum approach, J. Fluid Mech. **939**, A9 (2022).

[38] J. S. Hansen, B. D. Todd, and P. J. Daivis, Prediction of fluid velocity slip at solid surfaces, Phys. Rev. E **84**, 016313 (2011).

[39] C. L. Navier, Mémoire sur les lois du Mouvement des Fluides, Mémoires de l'Académie Royale des Sciences de l'Institut de France **6**, 389 (1823).

[40] L. Bocquet and J. L. Barrat, Flow boundary conditions from nano- to micro-scales, Soft Matter **3**, 685 (2007).

[41] C. Herrero, T. Omori, Y. Yamaguchi, and L. Joly, Shear force measurement of the hydrodynamic wall position in molecular dynamics, J. Chem. Phys. **151**, 041103 (2019).

[42] N. F. Carnahan and K. E. Starling, Equation of state for nonattracting rigid spheres, J. Chem. Phys. **51**, 635 (1969).

[43] T. Pöschel and T. Schwager, Event-driven molecular dynamics, in *Computational Granular Dynamics: Models and Algorithms*, 1st ed. (Springer, Berlin, 2005), pp. 135–189.

[44] M. G. Verbeek, Smoluchowski thermostat: A realistic introduction of the tangential momentum accommodation coefficient, Phys. Rev. E **81**, 046701 (2010).

[45] S. Varghese, J. S. Hansen, and B. D. Todd, Improved methodology to compute the intrinsic friction coefficient at solid-liquid interfaces, J. Chem. Phys. **154**, 184707 (2021).

[46] L. Gibelli, Velocity slip coefficients based on the hard-sphere Boltzmann equation, Phys. Fluids **24**, 022001 (2012).

[47] K. P. Travis and K. E. Gubbins, Poiseuille flow of Lennard-Jones fluids in narrow slit pores, J. Chem. Phys. **112**, 1984 (2000).

[48] A. Frezzotti, A particle scheme for the numerical solution of the Enskog equation, Phys. Fluids **9**, 1329 (1997).

[49] J. A. Thomas and A. J. H. McGaughey, Density, distribution, and orientation of water molecules inside and outside carbon nanotubes, J. Chem. Phys. **128**, 084715 (2008).

[50] S. Plimpton, Fast parallel algorithms for short-range molecular dynamics, J. Comput. Phys. **117**, 1 (1995).

[51] P. Spijker, A. J. Markvoort, S. V. Nedea, and P. A. J. Hilbers, Computation of accommodation coefficients and the use of velocity correlation profiles in molecular dynamics simulations, Phys. Rev. E **81**, 011203 (2010).